Physicochem. Probl. Miner. Process., 60(6), 2024, 195880

http://www.journalssystem.com/ppmp

Physicochemical Problems of Mineral Processing

ISSN 1643-1049

Analysis of bubble parameters in a fluidized flotation column with steel ball particles

Yingxiang Shi [1], Zhongkuan Wei [1,2], Huilin Xu [1], Fan Wu [1], Hang Gao [1], An Ping [1]

[1] China Coal Tianjin Design Engineering Co., Ltd., Tianjin 300120, China.

[2] School of Chemical Engineering and Technology, China University of Mining and Technology, Xuzhou, Jiangsu 221112, China

Corresponding author: cumt3344@163.com (Zhongkuan Wei)

Abstract: Examining the properties of bubble parameters within a three-phase system is crucial for enhancing and optimizing fluidized bed flotation column cells. This research focuses on the variations in primary bubble parameters within such columns, with the goal of offering a theoretical foundation for the advancement of fluidized bed flotation technology. The experiment utilized steel balls, tap water, and compressed air as the solid, liquid, and gas phases, respectively. Bubble parameters were measured directly using an electrical conductivity probe. Key factors influencing bubble size in the fluidized bed flotation column included the initial static bed height(H^*), superficial liquid velocity (U_L), superficial gas velocity (U_G), and reagent concentration. The study assessed how bubble size and gas holdup are distributed in the fluidization zone and identified how bubble parameters vary with different operating conditions. Findings show that incorporating steel ball particles in the fluidization zone significantly improves bubble stability, reduces the variability of bubble size, and ensures a more consistent bubble distribution. Proper selection of filling particles and accurate bed height adjustment can notably enhance the local gas holdup within the bed. Additionally, it has been found that local gas holdup increases rapidly when the liquid-to-gas velocity ratio drops below a certain threshold.

Keywords: bubble parameters, fluidized bed, flotation column cell

1. Introduction

The current investigation focuses on a three-phase flotation column, which consists of a bed of steel balls suspended in a flowing medium. This medium is composed of co-current compressed air and tap water, serving as the gas and liquid phases, respectively. Three-phase fluidization systems have numerous industrial applications, including in the fields of metallurgy, biochemical, chemical, and petrochemical production. The characteristics of three-phase beds have been extensively applied in studies across chemical, physical, and biochemical domains (Han et al., 2023a; Sur and Mukhopadhyay, 2017; Reese et al., 1999; Jena et al., 2008). It is well established that parameters such as gas holdup, bubble surface area flux, superficial gas velocity, and bubble size play crucial roles in influencing flotation and the associated particle transport and collection processes (Cheng et al., 2018; Panjipour et al., 2022; Rajapakse et al., 2022; Wang et al., 2016). Systematic investigations into flotation processes have been conducted. For instance, computational fluid dynamics (CFD) has been used to model these processes (Wang et al., 2018). Additionally, a CFD model has been developed to study gas holdup and bubble hydrodynamics within gas-liquid-solid flotation columns (Sarhan et al., 2017). Ravichandran and colleagues optimized gas parameters to enhance gas holdup and improve flotation performance (Zhang et al., 2024). Bubble characteristics in flotation columns are typically quantified using instruments or direct visualization techniques. Ityokumbul et al. estimated bubble sizes in flotation columns through a non-iterative method (Ityokumbul et al., 1995). Other researchers employed a bubble size analyzer at the base of the apparatus to measure bubble sizes via image analysis (Seger et al., 2019). The impact of frother concentration on bubble size has also been investigated (Karakashev et al., 2024; Pan et al., 2022). Bubble size is a critical parameter for gas distribution in flotation size n, significantly affecting flotation

DOI: 10.37190/ppmp/195880

efficiency (Han et al., 2023b; Han et al., 2022; Tao, 2022). Consequently, bubble parameter is a key factor in assessing the performance, scaling up, and designing of three-phase flotation columns.

Given the extensive application of gas-liquid-solid fluidized bed systems in contemporary industrial production (Abt et al., 2023; Liu et al., 2020), the experimental setup examined in this work involves a novel fluidized flotation column with uniform energy dissipation designed for coal flotation. This system aims to enhance the bubble-particle collision efficiency, improve the recovery of fine particles, and reduce energy consumption (Chen et al., 2023; Pan et al., 2018; Finch et al., 2006). It is positive established that an optimal bubble diameter distribution is crucial for achieving high flotation efficiency (Zhu et al., 2021). The target of this work is to investigate the characteristics and changes of bubble size during the flotation process in the fluidized bed flotation column cell. The findings from this research are anticipated to contribute to the broader understanding and development of fluidized bed flotation column cell-related studies.

In this study, experiments were carried out to examine the influence of U_L, U_G, H^*, and frother concentration on bubble parameters within the fluidized flotation column cell.

2. Experimental

2.1. Experimental setup

Fig. 1 presents a schematic of the experimental setup. The fluidized flotation column cell is constructed from Plexiglas, measuring 2.2 meters in height and 0.05 meters in internal size. Positioned 0.1 meters above the column's base, a porous plate with a 5 μm pore size and 0.01-meter thickness plays a crucial role in evenly dispersing gas. Water circulation within the flotation column is maintained by a liquid pump, with an electromagnetic flowmeter used to measure the circulating water's velocity. Compressed air is introduced at the column's base, with a rotameter employed to measure gas velocity. Above the gas disperser, a fixed bed composed of 0.03-meter glass balls is situated. A perforated stainless-steel plate with a 0.001-meter aperture and 25.47% porosity ensures the uniform distribution of gas and liquid while also supporting the steel ball particles. Bubble generation in the fluidized bed is monitored using a bubble measuring system through taps specifically designed on the column.

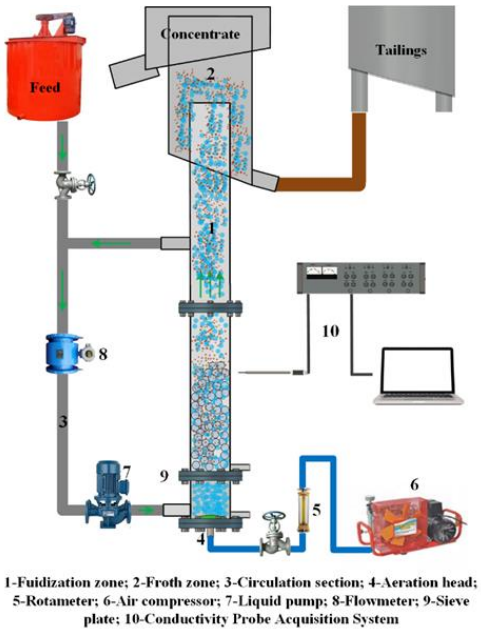

Fig.. 1. Analytical diagram of the experimental structure

The Sauter mean size (d_{32}) is commonly employed to characterize bubble size in multiphase flow systems (Wang et al., 2020). In this study, the bubble size is utilized as an equivalent representation of the d_{32}.

$$d_{32} = \frac{\sum_{i=1}^{n} d_i^3}{\sum_{i=1}^{n} d_i^2} \tag{1}$$

In this work, the bubble size was measured using the BVW multi-channel instrument, illustrated schematically in Fig. 2a. A conductivity probe was inserted into the fluidized flotation column cell through a designated hole. Bubbles moving upward were punctured successively by electrodes P_a and P_b, leading to changes in conductance values and resulting in variations in voltages (V_a, V_b) as depicted in Fig.. 2b. These voltage changes were automatically recorded by a computer. Subsequently, the d32 of the bubbles was calculated by commercial software based on the recorded voltage signals.

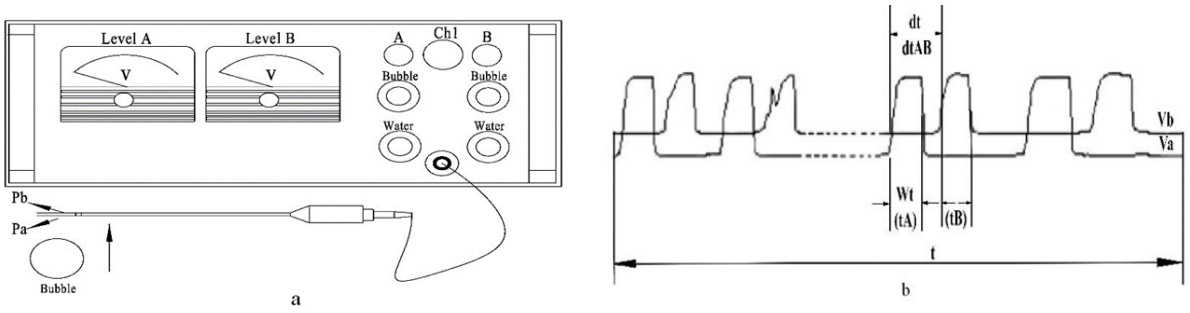

Fig. 2. Diagram of the bubble parameter testing system

Using the bed pressure drop method to calculate the local gas holdup in the fluidized zone, the following formula is used for the local gas holdup calculation (Jiang et al., 2023):

$$\frac{\Delta P}{g\Delta H} = \rho_l \varepsilon_l + \rho_g \varepsilon_g + \rho_s \varepsilon_s \tag{2}$$

$$\varepsilon_l + \varepsilon_g + \varepsilon_s = 1 \tag{3}$$

$$\varepsilon_s = \frac{M_s}{\rho_s A \Delta H} \tag{4}$$

where ΔP is the pressure drop in the turbulent regulated particle fluidized bed, the gas holdup calculation formula (4-4) is derived by converting Eqs. (2), (3), and (4):

$$\varepsilon_g = \frac{\frac{\Delta P}{g\Delta H} - \rho_l + \varepsilon_s(\rho_l - \rho_s)}{\rho_g - \rho_l} \tag{5}$$

2.2. Experimental procedure

The experiment was carried out under standard atmospheric pressure (101.320 Kpa) with the laboratory room maintained at a temperature of 20±1 °C. Table 1 outlines the experimental parameters. Compressed air served as the gas phase, tap water as the liquid phase, and steel ball particles as the solid phase. The H*s were set at 0.234 m, 0.259 m, 0.286 m, 0.314m, 0.340 m, and 0.377 m, respectively. To achieve these heights, specific amounts of solid particles were measured and then added directly into the flotation column. The water level in the column was kept above the circulating pipe to facilitate circular flow via the pump's action. Subsequently, the compressor introduced air into the column. The system stabilized within approximately 3-4 minutes. U_L and U_Gs were adjusted and measured using an electromagnetic flowmeter and an axe flowmeter, respectively. Test data were collected for various H*s, U_Gs, U_Ls, and frother concentrations.

Table 1. Details of experimental parameter ranges.

(1) Properties of solid materials			
Experimental materials	Density (g*cm^{-3})	Particle size (mm)	Free settling terminal velocity (m/s)
Steel ball	7.8	3.0/4.0/5.0	0.7024
(2) Properties of medium of fluidization			
	Medium Density (g*cm^{-3})		Kinematic viscosity (10^{-5} Pa·s)
Water	0.998		100.86
Air	0.00113		1.73

3. Results and discussion

3.1. Effect of H^* on bubble size

Fig. 3 illustrates how bubble size varies with different H^*s and superficial gas velocities, while keeping the U_L constant. It can be seen that the H^* significantly influences the bubble size. The Fig. clearly shows that as the H^* increases, the bubble size decreases. When the static bed height reaches 0.286 m, the bubble size is at its minimum. Increasing the H^* extends the duration of the through-fluidized region and increases the contact area. This expanded contact area boosts the likelihood of collisions, which promotes bubble breakup and thereby reduces the bubble size.

When the H^* varies between 0.286 m and 0.308 m, the bubble size increases with the bed height. This happens because larger fluidized regions encourage bubble coalescence. However, the change in bubble size becomes less noticeable when the H^* goes beyond 0.308 m. At this point, bubble breakage and coalescence processes reach a relative equilibrium. Cho and Laskowski suggested that bubble size could be influenced by bubble coalescence and/or breakage (Cho and Laskowski, 2002). In this investigation, the H^* may affect bubble coalescence and breakage.

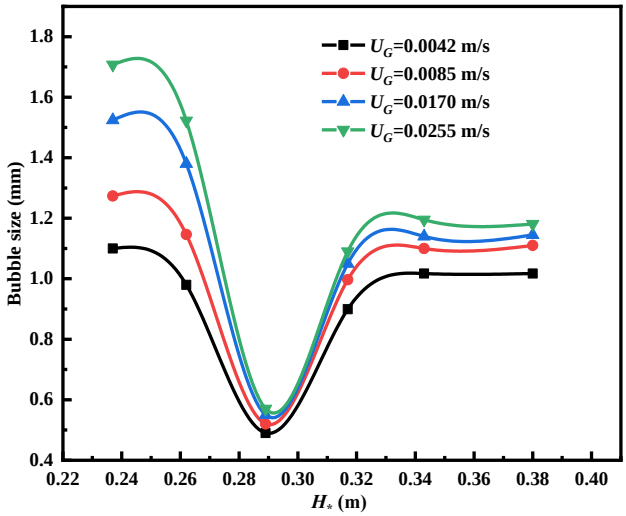

Fig. 3. Bubble size as a function of H^* at different U_G when U_L = 0.226 m/s

3.2. Effect of changes in U_G on bubble size

Fig. 4 shows how bubble size varies with U_G at different superficial liquid velocities, with the H^* consistently set at 0.286 m. The analysis of the Fig. reveals that bubble size is affected by U_L. Under conditions of low U_L, the bubble size decreases as U_G increases. Han et al. (2023c) observed that at relatively low liquid velocities, a higher U_G leads to a smaller bubble size. When the U_L exceeds 0.226 m/s, the bubble size trend displays a gradual increase with rising U_G, suggesting more frequent bubble coalescence.

However, Cho & Laskowski (2002) and Quinn et al. (2007) observed that at elevated gas velocities, a significant quantity of microbubbles is produced, and bubble coalescence is prevented. Thus, the occurrence of bubble coalescence at high gas velocities may be influenced by the specific experimental conditions. The Fig. demonstrates that bubble size tends to increase with rising air velocity, indicated by lower slopes, while bubble size decreases with increasing superficial air velocity, which is represented by steeper slopes. The U_L is a critical factor in this process.

3.3. Effect of U_L on bubble size

Fig. 5 illustrates how bubble size varies with U_L at a constant H^* for different superficial gas velocities. The data reveal that, for all compressed air velocities, the bubble size initially decreases before increasing as the U_L rises. Analysis of Fig. 5 leads to several key observations. Specifically, when the liquid velocity is below 0.266 m/s, lower compressed air velocities produce larger bubbles. Furthermore, the decrease in bubble size with increasing U_L is more noticeable at lower air velocities

compared to higher ones. This suggests that at lower U_Gs, the bubble size exhibits less variation with increasing liquid velocity. As the U_L grows, the turbulence in the fluidized flotation column cell increases, which enhances bubble breakup and results in smaller bubble sizes.

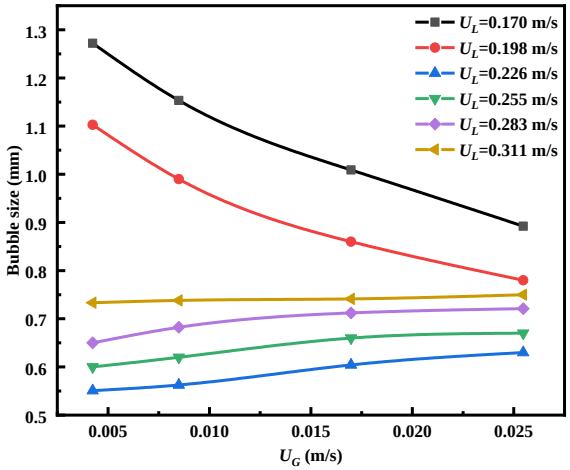

Fig. 4. Variation of bubble size with U_G for different liquid velocities at H^*=0.286 m

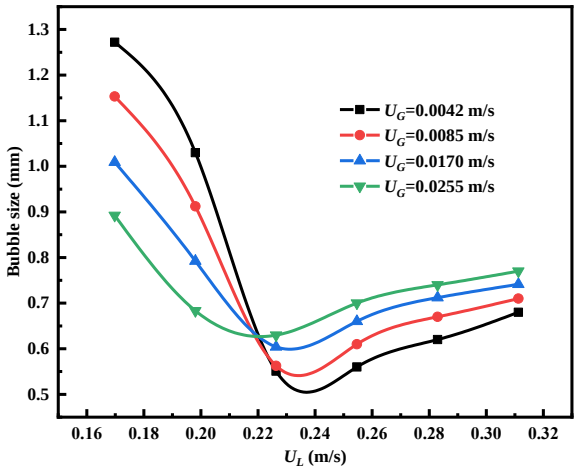

Fig. 5. Bubble size as a function of U_L at different U_Gs when H^*=0.286 m

Prakash and Majumder arrived at comparable findings (Prakash and Majumder, 2020). When the U_L surpasses 0.266 m/s, the size of bubbles tends to increase with rising U_L across all superficial gas velocities. Increased water velocities enhance the bed's porosity, which reduces the collision force between the steel balls and the bubbles. This reduction weakens the shear impact on the bubbles, leading to larger bubble sizes. Additionally, as depicted in Fig.. 5, bubbles formed at lower superficial gas velocities generally exhibit smaller sizes compared to those formed at higher U_Gs.

3.4. The role of reagent on bubble size

In this work, sec-octyl alcohol is employed as a frother to investigate its impact on bubble size, as illustrated in Fig.. 6. The Fig. shows that with a U_L of 0.226 m/s and an H^* of 0.286 m, an increase in frother concentration results in a reduction of bubble size across all U_Gs. Additionally, Fig.. 6 reveals that bubble size is less affected by frother concentration at lower superficial gas velocities compared to higher gas velocities. Initially, the bubble size decreases with rising frother concentration, eventually reaching a stable size after surpassing a critical frother concentration. Frother agents enhance the surface activity of bubbles and reduce coalescence, leading to smaller bubble sizes. Once the frother concentration exceeds the critical threshold, further increases have minimal effects on bubble coalescence suppression, resulting in relatively constant bubble diameters (Zhu et al., 2021). Cho and Laskowski (2006) have observed that at lower frother concentrations, bubble sizes are significantly

larger, suggesting that coalescence predominantly influences bubble size. According to Fig.. 6 and Cho's observations, it is clear that bubble coalescence at elevated gas velocities is more pronounced compared to lower gas velocities.

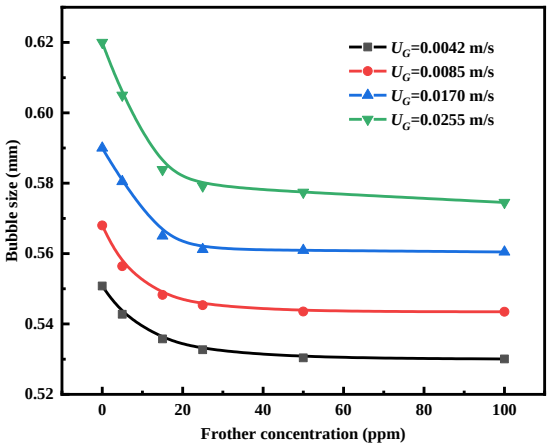

Fig. 6 Bubble size as a function of reagent concentration at different U_Gs when H^*=0.286m and U_L=0.226m/s

3.5. Turbulence modulates the effect of particle properties on gas holdup

Fig. 7 depicts how gas holdup varies within the fluidized column region of a bed filled with steel balls of different sizes, with a U_L of 0.169 m/s and an H^* of 0.290 m. The data shows that gas holdup in this region increases as the U_G rises. For a given set of experimental conditions, the local gas holdup in the fluidized bed for various particle sizes also shows an upward trend with increasing U_G. This rise in velocity leads to a higher volume of gas being introduced into the fluidized bed each second, which in turn causes a significant increase in local gas holdup within the fluidized region.

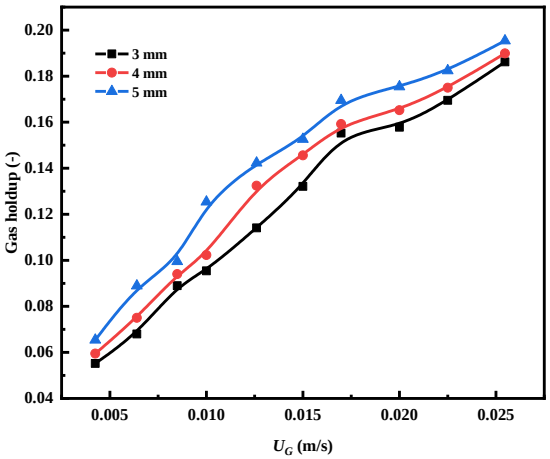

Fig. 7. Gas holdup as a function of U_G for different sizes of steel ball particles. (U_L=0.169 m/s，H^*=0.290 m)

Fig. 7 illustrates that, when maintaining constant gas velocity and varying only the particle size of the filling material, the gas holdup tends to rise with larger particle sizes. Nonetheless, the extent of this increase is relatively modest. Analyzing the general trend shown in Figs. 4-7 and comparing the data points, it becomes evident that while there is a general rise in gas holdup with increasing particle size, the variations in local gas holdup within the fluidized bed remain minimal across different particle sizes.

3.6. Effect of H^* on gas holdup

Fig. 8 illustrates how gas holdup changes with U_G across various H^*s, utilizing 3 mm steel beads as packing material and a U_L of 0.226 m/s. The Fig. demonstrates that, for each static bed height, an increase in gas flow rates leads to a higher local gas holdup within the fluidized bed column region.

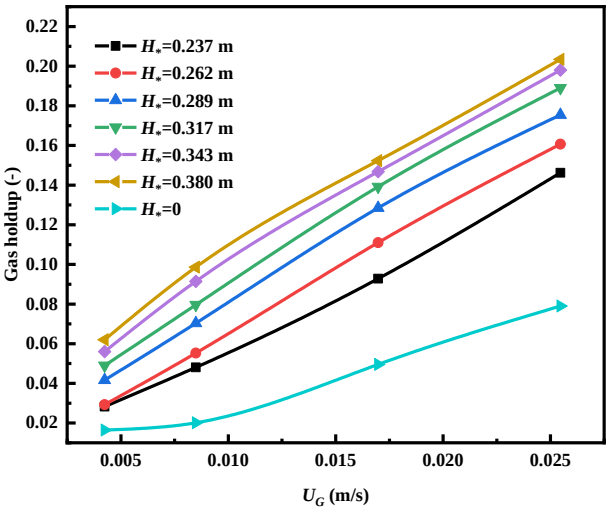

Fig. 8. Variation of gas holdup with U_G for different H*s (U_L=0.226 m/s)

Table 2. Data on the variation of gas holdup under different H* conditions

U_G	H_* (m)							Maximum percentage
(m/s)	0.000	0.237	0.262	0.289	0.317	0.343	0.380	Difference (%)
0.0042	0.016	0.028	0.029	0.042	0.043	0.0500	0.051	210.41
0.0085	0.020	0.048	0.055	0.070	0.080	0.091	0.099	391.16
0.0170	0.050	0.093	0.111	0.129	0.140	0.147	0.152	207.43
0.0255	0.079	0.146	0.161	0.175	0.180	0.181	0.186	135.32

Fig. 8 illustrates that as the U_G is increased, there is a corresponding rise in gas holdup. However, the extent of this increase differs depending on the H*. At lower H*s, the rate at which gas holdup grows with increasing U_G is slower. In contrast, at higher H*s, gas holdup shows a more rapid increase as the U_G rises.

Table 2 provides data derived from Fig.. 8, illustrating that the local gas holdup in the column cell increases as both gas velocity and the H* rise. The final column of the table shows the variation in local gas holdup with static bed height across different U_G scenarios. Analysis of the numerical data reveals that, at higher U_Gs, the change in bubble size with H* is relatively minor, while at lower gas velocities, the variation is more pronounced. The packed bed has a considerable impact on bubble size, with observed differences ranging from about 135% to nearly 400%.

This section explores the experimental study of how the "retention" effect of the initial static bed influences the gas phase. Fig. 9 depicts the gas holdup in the upper region of the three-phase fluidized bed system. For example, at X=0, it shows the gas holdup within the fluidized bed column cell, while at X=0.10 m, it represents the gas holdup 0.10 meters vertically above this area. The Fig. reveals that, under constant gas and liquid velocities, gas holdup values are higher closer to the three-phase fluidized bed area, varying with different H*s. As the vertical distance from the fluidized bed column cell increases, the gas holdup in the gas-liquid two-phase fluidized zone gradually decreases and eventually reaches a stable value.

Fig. 9 illustrates that as the H* rises, the retention effect of the fluidized bed column cell on gas holdup becomes more pronounced. The dashed auxiliary lines in the Fig. show that greater static bed heights are associated with larger fluctuations in gas holdup values along the vertical axis. The term "gas retention rate" is used to denote the percentage change in gas holdup in this vertical direction. The data depicted indicate that as the static bed height increases, so does the gas retention rate. Calculations from the data demonstrate that the gas retention rate varies between a low of 6.67% and a high of 27.36%. Overall, the inclusion of the packed bed significantly improves the local gas holdup within the fluidized bed column cell.

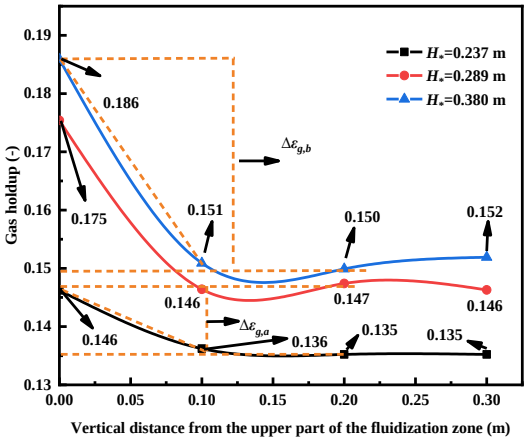

Fig. 9. Variation of gas holdup as a function of vertical direction for different H^*. (U_L=0.226 m/s, U_G=0.0255 m/s)

3.7. Effect of U_L and U_G synergy on gas holdup ratio

Fig. 10 depicts how gas holdup varies with the liquid-to-gas velocity ratio under various U_L conditions, with an H^* of 0.290 meters and 3 mm steel beads used as packing particles. The graph reveals two distinct patterns in the behavior of gas holdup. Initially, as the liquid-to-gas ratio decreases, the increase in gas holdup is gradual. However, when the ratio drops below a specific threshold, gas holdup rises sharply. This indicates the presence of a critical liquid-to-gas velocity ratio; below this threshold, there is a conspicuous increase in gas holdup within the fluidized bed. This behavior notably improves the local gas holdup in the fluidized bed column cell with steel beads, which is advantageous for flotation processes.

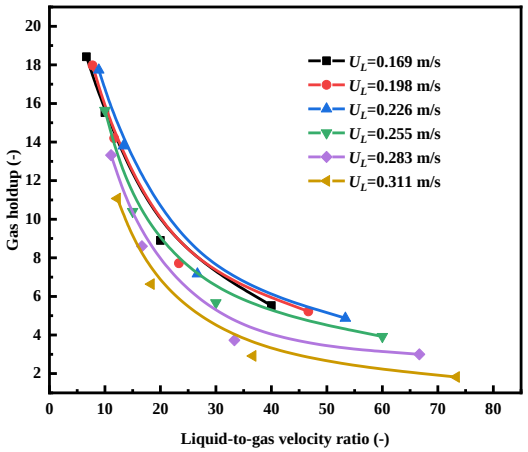

Fig. 10. Gas holdup as a function of liquid-gas velocity ratio at different U_Ls. (H^*=0.290 m)

Given the limited experimental data, continuous curves can be constructed by selecting several broad ranges of liquid-to-gas velocity ratios and their corresponding gas holdup values. For each liquid velocity, the critical liquid-to-gas velocity ratio can be determined using the method illustrated in Fig. 10. In subsequent flotation experiments, we will use this approach to determine suitable values for superficial liquid and gas velocities.

Through the aforementioned study and analysis, the significance of the liquid-to-gas velocity ratio in enhancing the gas performance of fluidized beds is evident. Optimal ratios can effectively increase local gas holdup in fluidized beds, improve gas performance in the fluidized area, and consequently enhance separation efficiency in flotation unit.

3.8. Relationship between bubble size and gas holdup for mineralization process

Fig. 11 illustrates how gas holdup varies with bubble size as the H^* changes under various gas velocity conditions, while maintaining a U_L of 0.226 m/s. The diagram indicates that an H^* of 0.290 m serves as

a critical threshold, separating two distinct patterns in the relationship between gas holdup and bubble size. For static bed heights below 0.290 m, increasing the bed height leads to a reduction in bubble size, which in turn raises gas holdup as the bubble size decreases. On the other hand, for static bed heights greater than approximately 0.290 m, further increases in bed height initially cause the bubble size to grow. During this phase, gas holdup increases with the growing bubble size until both the bubble size and gas holdup reach a steady state, with only minor fluctuations occurring with additional increases in static bed height.

Fig. 12 depicts how gas holdup varies with bubble size as water velocity changes under different U_G conditions, with a H^* of 0.290 m. The data clearly reveals a distinction at a water velocity of 0.226 m/s, separating two distinct patterns in the relationship between gas holdup and bubble size. For U_Ls

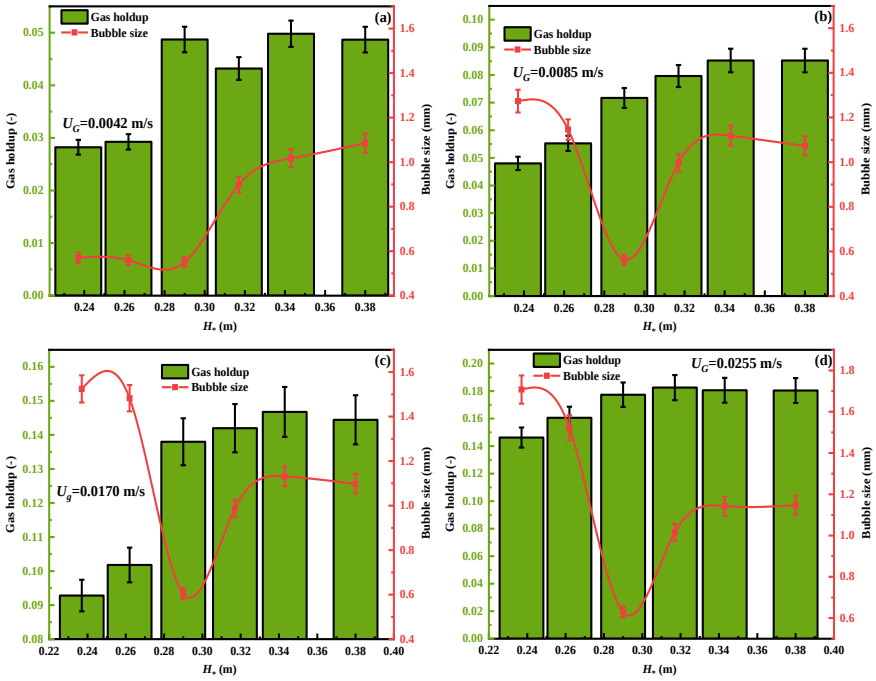

Fig. 11. Gas holdup as a function of bubble size at different U_G. (U_L=0.226 m/s)

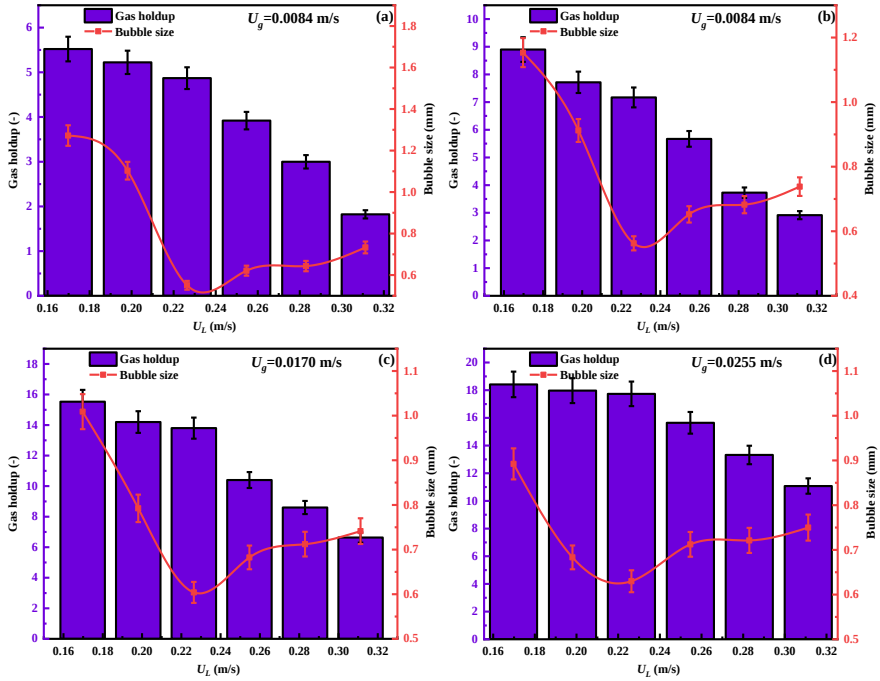

Fig. 12. Variation of gas holdup with bubble size for different U_Gs (U_L=0.226 m/s)

below 0.226 m/s, an increase in water velocity leads to enhanced bubble breakup, which results in a reduction of the average bubble size and a decrease in gas holdup. On the other hand, for U_L above 0.226 m/s, higher apparent water velocities promote bubble coalescence, increasing the average bubble size, although gas holdup continues to decrease as bubble size increases.

Fig. 13 illustrates how gas holdup correlates with bubble size as the volume of gas introduced into the fluidized bed varies, with an H^* of 0.290 m and different U_Ls. The diagram reveals two distinct patterns regarding the relationship between gas holdup and bubble size under varying water velocity conditions: at U_Ls below 0.226 m/s, a larger average bubble size tends to hinder the growth of gas holdup; conversely, when the water velocity surpasses 0.226 m/s, gas holdup increases as bubble size grows.

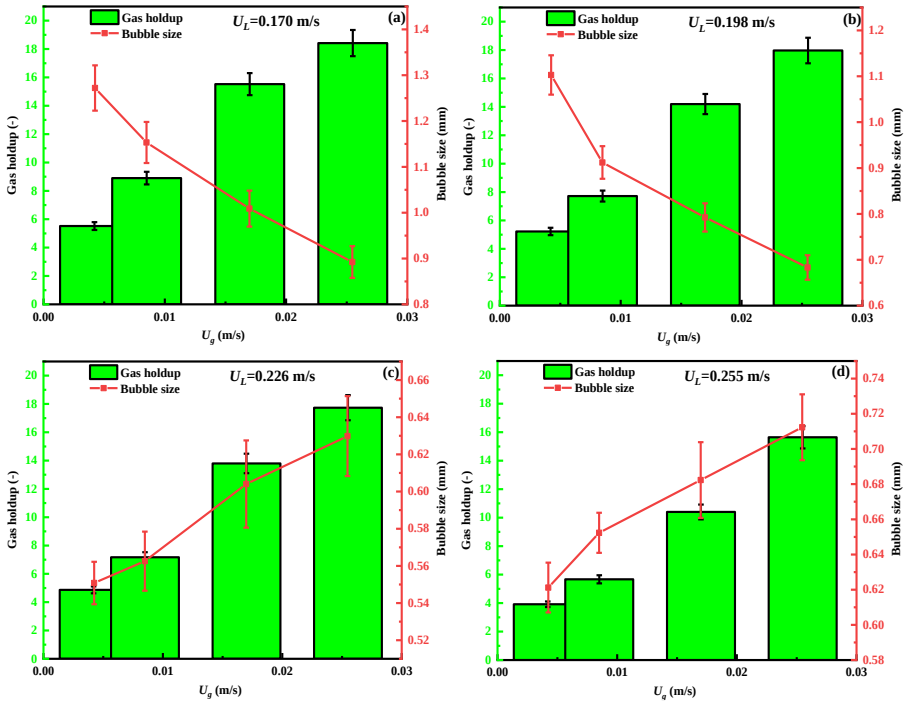

Fig. 13. Variation of gas holdup with bubble size for different U_Ls (H^*=0.290 m)

4. Conclusions

Experiments were performed to examine bubble parameters within a fluidized flotation column cell. The results indicated that bubble size varies with the height of the static bed: initially decreasing as the static bed height increases, but subsequently increasing with further height increments. The U_G exhibits a dual impact on bubble size depending on the U_L. Specifically, when the U_L is low, the bubble size diminishes with rising U_G. Conversely, at higher liquid velocities, the bubble size increases with greater U_G. Additionally, the research demonstrated that bubble size decreases with rising U_L up to a certain point, after which the size begins to increase if the liquid velocity surpasses a critical threshold. Frother concentration significantly affects bubble size, which consistently decreases as frother concentration increases across all scenarios. However, when frother concentration exceeds a critical level, the bubble size stabilizes.

Furthermore, under specific experimental conditions, a positive correlation exists between the size of the packed particles, the H^*, and the increase in gas holdup. When experimental conditions remain constant, a higher H^* leads to a greater local gas holdup in the fluidization zone, and the rate at which gas holdup increases with gas velocity becomes faster. The initial static bed exerts a retention effect on the gas phase, resulting in a higher local gas holdup in the fluidized flotation column cell system compared to the two-phase system. This retention effect becomes more pronounced with a higher initial static bed. For a given liquid velocity, an optimal liquid-to-gas velocity ratio exists when the H^* is fixed. If this ratio falls below the optimal level, gas holdup in the fluidized bed rises quickly, thereby significantly improving the local gas holdup in the fluidization zone.

This study explored and analyzed the parameters of bubbles produced in a fluidized flotation column cell under different experimental conditions. The findings offer valuable insights for the advancement and development of three-phase fluidized flotation column technology.

Acknowledgments

This paper is supported by the Fundamental Research Funds for the National Natural Science Foundation of China (Grant No.51674258 and No.51874304) and we also want to thank the support of the Key Science and Technology Projects of China National Coal Group Corp (20231CY003).

References

ABT, M., FRANZREB, M., JESTÄDT, M., TSCHÖPE, A., 2023. *Three-phase fluidized bed electrochemical reactor for the scalable generation of hydrogen peroxide at enzyme compatible conditions*, Chem. Eng. J., 476, 146465.

CHEN, P., LI, Y., HAN, J., JING, L., ZHANG, Z., LI, Y., 2023. *Hydrodynamics of fluidized bed flotation column with a homogeneous binary mixture of steel balls*. Powder. Technol. 429, 118920.

CHENG, Y., MIN, F., LI, H., CHEN, J., FU, X., 2018. *Effect of reagent interaction on froth stability of coal flotation*. Fuel. 318, 123417.

CHO, Y. S., LASKOWSKI, J. S., 2002. *Effect of flotation frothers on bubble size and foam stability*. Int. J. Miner. Proces., 64, 69-80.

FINCH, J. A., GELINAS. S., MOYO., P., 2006. *Frother-related research at mcgill university*. Miner. Eng.,19, 726-733.

HAN, J., CHEN, P., LIU, T., LI, Y., 2023a. *Research and application of fluidized flotation units: A review*. J. Ind. Eng. Chem. 126, 50-68.

HAN, J., FANG, J., YANG, T., CHEN, P., LIU, T., LI, Y., 2023b. *Particle motion analysis of a new three-phase fluidized bed flotation column with glass sphere particle*s. Adv. Powder. Technol., 34, 104265.

HAN, J., LI, Y., CHEN, P., 2023c. *A study of bubble size/shape evolution in microbubble countercurrent contacting flotation column*, Asia-Pac. J. Chem. Eng. 18, e2865.

HAN, J., LIU, T., LI, Y., CHEN, P., YIN, M., MA, M., EVANS, G. M., 2022. *Bed hydrodynamics of a new three-phase fluidized bed flotation column with steel ball particles.* Miner. Eng. 184, 107669.

ITYOKUMBUL, M. T., SALAMA, A. I. A., TAWEEL, A. M. A., 1995, *Estimation of bubble size in flotation columns.* Miner. Eng., 8, 77-89.

JIANG, F., YAN, S., QI, G., LI, X., 2023. *Particle distribution and pressure drop in a horizontal two-pass liquid-solid circulating fluidized bed heat exchanger*, Powder. Technol., 416, 118210.

JENA, H. M., ROY, G. K., MEIKAP, B. C., 2008. *Prediction of gas holdup in a three-phase fluidized bed from bed pressure drop measurement*. Chem. Eng. Res. Des. 8, 1301-1308.

KARAKASHEV, S. I., IVANOVA-STANCHEVA, D. S., GROZEV, N. A., MIRCHEVA, K. M., 2024. *Behavior of froth in absence and presence of particles*, Miner. Eng., 2024, 12, 108715.

LIU., T, LI. Y., HE, S., CHEN, P., LI, Z., 2020. *Optimization of air parameters in a three-phase fluidized bed flotation column*. Powder Technol., 373, 242-253.

SUR, D. H., MUKHOPADHYAY, M., 2017. *Process aspects of three-phase inverse fluidized bed bioreactor: A review*. J. Environ. Chem. Eng. 5, 3518-3528.

REESE, J., SILVA, E. M., YANG, S., FAN, L. -S., 1999. *Industrial Applications of Three-Phase Fluidization Systems*. Fluidization Solids Handling & Processing. 582-682.

PAN, Y., BOURNIVAL, G., ATA, S., 2022. *Foaming behaviour of frothers in the presence of PAX and salt,* Miner. Eng., 2022, 178, 107405.

PAN, H., LI, Y., LI., N., GAO. F., FU, X., ZHU, R., EVANS, G. M., 2018. *Study on gas holdup in a fluidized flotation column from bed pressure drop*. Energ. Source. Part. A., 40, 1693-1700.

PANJIPOUR, R., KARAMOOZIAN, M., ALBIJANIC, B., 2021. *Investigations of gas holdup, interfacial area of bubbles and bubble size distributions in a pilot plant flotation column*. Miner. Eng. 164, 106819.

PRAKASH, R., MAJUMDER, S. K., 2020. *Effect of particle size and concentration on bubble size distribution and aspect ratio in a counter-current microstructured bubble column*. J. Ind. Eng. Chem., 90, 105-116.

QUINN, J. J., KRACHT, W., GOMEZ, C. O., GAGNON, C., FINCH, J. A., 2007. *Comparing the effect of salts and frother (mibc) on gas dispersion and froth properties.* Miner. Eng., 20, 1296-1302.

RAJAPAKSE, N., ZARGAR, M., SEN, T., KHIADANI, M., 2022. *Effects of influent physicochemical characteristics on air dissolution, bubble size and rise velocity in dissolved air flotation: A review*. Sep. Purif. Technol., 289, 120772.

SARHAN, A. R., NASER, J., BROOKS, G., 2017, *Cfd analysis of solid particles properties effect in three-phase flotation column,* Sep. Purif. Technol. ,185, 1-9.

SEGER M.A., OLIVEIRA, C., RODRIGUES, R. T., 2019. *Development of a laboratory-scale flotation column with inlet bubble size measurement*. Miner. Eng., 142, 105936.

TAO, D., 2022. *Recent advances in fundamentals and applications of nanobubble enhanced froth flotation: A review,* Miner. Eng., 183, 107554.

WANG, B., YANG, G., TIAN, H., LI, X., YANG, G., SHI, Y., ZHOU, Z., ZHANG, F., ZHANG, Z., 2020. *A new model of bubble Sauter mean diameter in fine bubble-dominated columns*, Chem. Eng. J., 393, 124673.

WANG, G., GE, L., MITRA, S., EVANS, G. M., JOSHI, J. B., CHEN, S.Y., 2018, *A review of cfd modelling studies on the flotation process.* Miner. Eng., 127, 153-177.

WANG, G., NGUYEN, A. V., MITRA, S., JOSHI, J. B., JAMESON, G. J., EVANS, G. M., 2016. *A review of the mechanisms and models of bubble-particle detachment in froth flotation*. Sep. Purif. Technol. 170, 155-172.

ZHANG Z., FANG J., JING L. *The separation of fine minerals in the synergy between the vertical fluidization section and inclined channels of the Reflux Classifier*. Asia-pacific Journal of Chemical Engineering, 2024, 19(1).

ZHU, H., ZHU, J., MIN, F., VALDIVIESO, A. L., CORONA, A. M. A., Wang, H., 2021. *Effect of frother addition mode on coal flotation in downflow flotation column.* J. Clean. Prod. 278, 123844.